Flexural wave band gaps in locally resonant thin plates with periodically attached spring–mass resonators

2012 J. Phys. D: Appl. Phys. 45 195401

(http://iopscience.iop.org/0022-3727/45/19/195401)

IOP PUBLISHING JOURNAL OF PHYSICS D: APPLIED PHYSICS

J. Phys. D: Appl. Phys. **45** (2012) 195401 (12pp) doi:10.1088/0022-3727/45/19/195401

Flexural wave band gaps in locally resonant thin plates with periodically attached spring–mass resonators

Yong Xiao[1,2], **Jihong Wen**[1,2] **and Xisen Wen**[1,2,3]

[1] Institute of Mechatronical Engineering, and MOE Key Laboratory of Photonic and Phononic Crystals, National University of Defense Technology, Changsha 410073, People's Republic of China
[2] Laboratory of Science and Technology on Integrated Logistics Support, National University of Defense Technology, Changsha 410073, People's Republic of China

E-mail: wenxs@vip.sina.com

Received 24 November 2011, in final form 22 March 2012
Published 20 April 2012
Online at stacks.iop.org/JPhysD/45/195401

Abstract
The authors study the propagation of flexural waves in a locally resonant (LR) thin plate made of a two-dimensional periodic array of spring–mass resonators attached on a thin homogeneous plate. The well-known plane wave expansion method is extended to deal with such a plate system with a periodic array of lumped resonant elements. Explicit matrix formulations are developed for the calculation of complex band structures, in which the imaginary parts of Bloch wave vectors are displayed to quantify the wave attenuation performance of band gaps. It is found that resonance-type and Bragg-type band gaps coexist in the LR plate, and the bandwidth of these gaps can be dramatically affected by the resonant frequency of local resonators. In particular, a super-wide pseudo-directional gap can be formed by a combination of the resonance gap and Bragg gap; inside such a pseudo-gap, only a very narrow pass band exists. An explicit formula is further developed to facilitate the design of such a pseudo-gap. Finally, vibration transmission in finite LR plates is calculated using the finite element method. Vibration transmission gaps are observed, and the results are in good agreement with the band gap properties predicted by the complex band structures.

(Some figures may appear in colour only in the online journal)

1. Introduction

In the past few years, artificial periodic composites known as phononic crystals (PCs), consisting of a periodic array of elastic scatterers embedded in a host medium, have received considerable attention [1–3]. One of the most important properties of PCs is the so-called acoustic/elastic wave band gap: a frequency range where all acoustic/elastic waves cannot propagate through the periodic system. Such a unique property promises applications such as acoustic and mechanical wave filters, acoustic barriers, vibration isolators and design of transducers.

Earlier investigations on PCs generally concern band gaps based on the Bragg scattering mechanism. Such band gaps are called the Bragg-type gaps, appearing around frequencies governed by the Bragg condition $L = n(\lambda/2)$ ($n = 1, 2, 3, \ldots$), where L is the lattice constant of the periodic system, and λ is the wavelength of the waves in the host material. Bragg condition implies that, to achieve a Bragg gap in PCs, the structure period must be of the same order as the wavelength of the band-gap frequencies. Thus, it is difficult to engineer low-frequency Bragg gaps in PCs with a small structural dimension. Recently, in contrast, Liu *et al* proposed a locally resonant (LR) mechanism to form low-frequency band gaps [4]. They fabricated a type of LR PC containing an array of LR units. Resonance-type gaps were achieved in a frequency range two orders of magnitude lower than that given by the Bragg limit [4]. This pioneering work has led to an additional field of PCs in the last decade [5–14]. More recently, the study of LR PCs has been

[3] Author to whom any correspondence should be addressed.

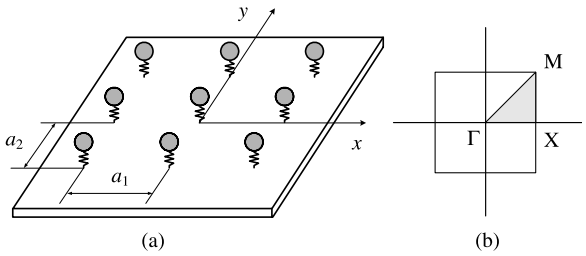

Figure 1. (*a*) Schematic diagram of a LR thin plate with a 2D periodic array of attached spring–mass resonators. (*b*) Corresponding first Brillouin zone of the periodic lattice. The grey area in (*b*) is the irreducible region of the Brillouin zone.

extended to a newly emerging field: acoustic metamaterials (AMs) [15–18]. AMs are generally regarded as materials with manmade microstructures that possess novel physical behaviour such as negative effective mass and/or modulus [19–21].

LR PCs and AMs are always fabricated by arrays of resonant microstructures embedded in a host medium. Such an idea can be implemented in the context of vibration control engineering, where various elastic structures such as rods, beams and plates are commonly used. Low-frequency resonance gaps can be achieved in these structures by mounting an array of resonant elements periodically to them. The idea has recently been validated theoretically and/or experimentally for rods [22], beams [23–25] and plates [9, 10, 12, 26–28]. However, only the plate case will be considered in this paper. The control of flexural vibration and wave propagation in elastic thin plates is of great importance in engineering since thin plates are typical structural elements of many engineering constructions, and flexural wave motion in thin plates can lead to undesirable vibration transmission and noise radiation [29]. The existence of flexural wave band gaps in LR plates provides a new idea for the vibration and wave propagation control of plates and plate-like structures [9, 12, 18].

In this paper, we examine flexural wave band gaps in a LR plate system consisting of a uniform thin plate with periodically attached spring–mass resonators. The well-known plane wave expansion (PWE) method [30, 31] is extended to treat such a periodic plate system containing lumped resonant elements (i.e. the spring–mass resonators), and to calculate the imaginary part of Bloch wave vectors that can be used to quantify the wave attenuation performance of band gaps. Vibration transmission in finite LR plates is further examined using the finite element method. The presence of vibration transmission gaps in finite LR plates confirms the existence of band gaps predicted by the PWE method.

2. Model and formulations

Consider an infinitely thin plate lying in the x–y plane with periodically attached resonators, as sketched in figure 1(*a*). Each resonator consists of a spring k_{R} and a mass m_{R}, which determine the resonant frequency of the resonator: $f_{\mathrm{R}} = (1/2\pi)(k_{\mathrm{R}}/m_{\mathrm{R}})^{1/2}$. In figure 1(*a*), the attachment point of a resonator can be denoted by a direct lattice vector [32]:

$$\boldsymbol{R} = \bar{m}\boldsymbol{a}_1 + \bar{n}\boldsymbol{a}_2, \tag{1}$$

where $\bar{m}$ and $\bar{n}$ are integers, $\boldsymbol{a}_1 = (a_{11}, a_{12})$ and $\boldsymbol{a}_2 = (a_{21}, a_{22})$ are basis vectors of the direct lattice. It should be pointed out that the formulations presented in this section can deal with various types of lattices, but in the numerical examples of this paper, we only examine the case of a rectangular lattice shown in figure 1(*a*); the basis vectors of the lattice are $\boldsymbol{a}_1 = (a_1, 0)$, $\boldsymbol{a}_2 = (0, a_2)$.

According to the classical theory of thin plates [29], the governing equation for the time-harmonic vibration of the plate–resonator coupled system shown in figure 1(*a*) can be written as

$$\begin{cases} D\left(\dfrac{\partial^2}{\partial x^2} + \dfrac{\partial^2}{\partial y^2}\right)^2 w_1(\boldsymbol{r}) - \omega^2 \rho h w_1(\boldsymbol{r}) \\ \quad = \displaystyle\sum_{\boldsymbol{R}} [f_1(\boldsymbol{R})\delta(\boldsymbol{r} - \boldsymbol{R})], \\ -\omega^2 m_{\mathrm{R}} w_2(\boldsymbol{R}) = f_2(\boldsymbol{R}), \end{cases} \tag{2}$$

with

$$\begin{cases} f_1(\boldsymbol{R}) = -k_{\mathrm{R}}[w_1(\boldsymbol{R}) - w_2(\boldsymbol{R})], \\ f_2(\boldsymbol{R}) = k_{\mathrm{R}}[w_1(\boldsymbol{R}) - w_2(\boldsymbol{R})]. \end{cases} \tag{3}$$

In equation (2), $D = Eh^3/12(1 - \nu^2)$ is the plate bending stiffness, ρ is the density of the plate material, h is the thickness of the plate, $\boldsymbol{r} = (x, y)$ denotes the location of points, $w_1(\boldsymbol{r})$ represents the transverse displacement of the plate, $w_2(\boldsymbol{R})$ is the displacement of the resonator mass at $\boldsymbol{R}$, $f_1(\boldsymbol{R})$ refers to the force applied to the plate by the spring at $\boldsymbol{R}$, $f_2(\boldsymbol{R})$ represents the force applied to the connected mass by this spring, and $\delta(\boldsymbol{r} - \boldsymbol{R})$ is a two-dimensional (2D) delta function defined as

$$\delta(\boldsymbol{r} - \boldsymbol{R}) = \delta(x - \boldsymbol{R}_x)\delta(y - \boldsymbol{R}_y). \tag{4}$$

In addition, it is worth noting that equation (2) is valid only if the thickness of the thin plate is small enough in comparison with the flexural wavelength of motion in the thin plate. An appropriate condition for the validity of the thin plate assumption is $h < \lambda_{\mathrm{P}}/6$ [29], where λ_{P} refers to the flexural wavelength, given by

$$\lambda_{\mathrm{P}} = \frac{2\pi}{k_{\mathrm{P}}} = \frac{2\pi}{(\rho h\omega^2/D)^{1/4}}. \tag{5}$$

Here, $k_{\mathrm{P}} = (\rho h\omega^2/D)^{1/4}$ represents the flexural wavenumber of the thin plate.

Due to the periodicity of the system, the displacement response of the plate can be written as

$$w_1(\boldsymbol{r}) = \sum_{\boldsymbol{G}} W_1(\boldsymbol{G}) \mathrm{e}^{-\mathrm{i}(\boldsymbol{k}+\boldsymbol{G})\cdot\boldsymbol{r}}, \tag{6}$$

where $\boldsymbol{k} = (k_x, k_y)$ is the Bloch wave vector (wave number), and $\boldsymbol{G}$ denotes the reciprocal-lattice vector [32], given by

$$\boldsymbol{G} = m\boldsymbol{b}_1 + n\boldsymbol{b}_2, \tag{7}$$

where m and n are integers, $\boldsymbol{b}_1 = (b_{11}, b_{12})$ and $\boldsymbol{b}_2 = (b_{21}, b_{22})$ are basis vectors of the reciprocal lattice, defined such that

$$\boldsymbol{a}_p \cdot \boldsymbol{b}_q = 2\pi\delta_{pq} \qquad (p, q = 1, 2). \tag{8}$$

For the rectangular array considered in figure 1(*a*), we have $\boldsymbol{b}_1 = (2\pi/a_1, 0)$, $\boldsymbol{b}_2 = (0, 2\pi/a_2)$.

Also note that the periodic condition implies that

$$\begin{cases} w_1(\boldsymbol{R}) = w_1(\boldsymbol{0})\mathrm{e}^{-\mathrm{i}\boldsymbol{k}\cdot\boldsymbol{R}}, \\ w_2(\boldsymbol{R}) = w_2(\boldsymbol{0})\mathrm{e}^{-\mathrm{i}\boldsymbol{k}\cdot\boldsymbol{R}}, \end{cases} \tag{9}$$

and the delta function suggests the following relation:

$$\sum_{\boldsymbol{R}} \mathrm{e}^{-\mathrm{i}\boldsymbol{k}\cdot\boldsymbol{R}}\delta(\boldsymbol{r}-\boldsymbol{R}) = \mathrm{e}^{-\mathrm{i}\boldsymbol{k}\cdot\boldsymbol{r}} \sum_{\boldsymbol{R}} \delta(\boldsymbol{r}-\boldsymbol{R}). \tag{10}$$

By substituting equations (9) and (10) into equation (2), we obtain the following equation:

$$\begin{cases} D\nabla^4 w_1(\boldsymbol{r}) - \omega^2\rho h w_1(\boldsymbol{r}) = \{-k_{\mathrm{R}}[w_1(\boldsymbol{0}) - w_2(\boldsymbol{0})]\} \\ \quad \mathrm{e}^{-\mathrm{i}\boldsymbol{k}\cdot\boldsymbol{r}} \sum\limits_{\boldsymbol{R}} \delta(\boldsymbol{r}-\boldsymbol{R}), \\ -\omega^2 m_{\mathrm{R}} w_2(\boldsymbol{0}) = k_{\mathrm{R}}[w_1(\boldsymbol{0}) - w_2(\boldsymbol{0})], \end{cases} \tag{11}$$

where $\nabla^4 = (\partial^2/\partial x^2 + \partial^2/\partial y^2)^2$.

Now introduce a function defined by $g(\boldsymbol{r}) = \sum_{\boldsymbol{R}} \delta(\boldsymbol{r}-\boldsymbol{R})$; due to the periodicity of the function it can be expressed in Fourier series as

$$g(\boldsymbol{r}) = \sum_{\boldsymbol{G}} \tilde{g}(\boldsymbol{G})\mathrm{e}^{-\mathrm{i}\boldsymbol{G}\cdot\boldsymbol{r}} \tag{12}$$

with

$$\begin{aligned} \tilde{g}(\boldsymbol{G}) &= \frac{1}{S}\iint_S g(\boldsymbol{r})\mathrm{e}^{\mathrm{i}\boldsymbol{G}\cdot\boldsymbol{r}}\,\mathrm{d}^2\boldsymbol{r} \\ &= \frac{1}{S}\iint_S \sum_{\boldsymbol{R}} \delta(\boldsymbol{r}-\boldsymbol{R})\mathrm{e}^{\mathrm{i}\boldsymbol{G}\cdot\boldsymbol{r}}\,\mathrm{d}^2\boldsymbol{r} = \frac{1}{S}, \end{aligned} \tag{13}$$

where $S = |\boldsymbol{a}_1 \times \boldsymbol{a}_2|$ is the area of the unit cell associated with the periodic lattice. Accordingly, we obtain the following relation:

$$\sum_{\boldsymbol{R}} \delta(\boldsymbol{r}-\boldsymbol{R}) = \frac{1}{S}\sum_{\boldsymbol{G}} \mathrm{e}^{-\mathrm{i}\boldsymbol{G}\cdot\boldsymbol{r}}. \tag{14}$$

Substituting equations (6) and (14) into equation (11) gives

$$\begin{cases} D[(\boldsymbol{k}+\boldsymbol{G})_x^2 + (\boldsymbol{k}+\boldsymbol{G})_y^2]^2 W_1(\boldsymbol{G}) - \omega^2\rho h W_1(\boldsymbol{G}) \\ \quad = (-k_{\mathrm{R}}/S)[w_1(\boldsymbol{0}) - w_2(\boldsymbol{0})], \\ -\omega^2 m_{\mathrm{R}} w_2(\boldsymbol{0}) = k_{\mathrm{R}}[w_1(\boldsymbol{0}) - w_2(\boldsymbol{0})]. \end{cases} \tag{15}$$

Note that

$$w_1(\boldsymbol{0}) = \sum_{\boldsymbol{G}} W_1(\boldsymbol{G}). \tag{16}$$

Inserting this into equation (15) yields

$$\begin{cases} D[(\boldsymbol{k}+\boldsymbol{G})_x^2 + (\boldsymbol{k}+\boldsymbol{G})_y^2]^2 W_1(\boldsymbol{G}) - \omega^2\rho h W_1(\boldsymbol{G}) \\ \quad = (-k_{\mathrm{R}}/S)[\sum\limits_{\boldsymbol{G}} W_1(\boldsymbol{G}) - w_2(\boldsymbol{0})], \\ -\omega^2 m_{\mathrm{R}} w_2(\boldsymbol{0}) = k_{\mathrm{R}}[\sum\limits_{\boldsymbol{G}} W_1(\boldsymbol{G}) - w_2(\boldsymbol{0})]. \end{cases} \tag{17}$$

To solve equation (17), we must truncate the infinite summation. If we choose $m, n = (-M, \ldots, M)$, the number of plane waves (W_1) used in the calculation is $N \times N = (2M+1)\times(2M+1)$. Therefore equation (17) can be expressed by a matrix formulation as

$$\left(\begin{bmatrix} DS[\boldsymbol{K}] + k_{\mathrm{R}}[\boldsymbol{U}] & -k_{\mathrm{R}}[\boldsymbol{P}] \\ -k_{\mathrm{R}}[\boldsymbol{P}^{\mathrm{T}}] & k_{\mathrm{R}} \end{bmatrix} - \omega^2 \begin{bmatrix} \rho h S[\boldsymbol{I}] & \boldsymbol{0} \\ \boldsymbol{0} & m_{\mathrm{R}} \end{bmatrix}\right) \times \begin{Bmatrix} \boldsymbol{W}_1 \\ w_2(\boldsymbol{0}) \end{Bmatrix} = \boldsymbol{0}, \tag{18}$$

where

$$[\boldsymbol{K}] = \begin{bmatrix} [\sum\limits_{j=x,y} (\boldsymbol{k}+\boldsymbol{G}_1)_j^2]^2 & 0 & \cdots & 0 \\ 0 & [\sum\limits_{j=x,y} (\boldsymbol{k}+\boldsymbol{G}_2)_j^2]^2 & \cdots & 0 \\ \vdots & \vdots & \ddots & \vdots \\ 0 & \cdots & 0 & [\sum\limits_{j=x,y} (\boldsymbol{k}+\boldsymbol{G}_{N\times N})_j^2]^2 \end{bmatrix}, \tag{19}$$

$$[\boldsymbol{P}] = \begin{bmatrix} 1 \\ 1 \\ \vdots \\ 1 \end{bmatrix}_{N^2\times 1}, \qquad [\boldsymbol{U}] = [\boldsymbol{P}\boldsymbol{P}^{\mathrm{T}}],$$

$$[\boldsymbol{I}] = \begin{bmatrix} 1 & 0 & \cdots & 0 \\ 0 & 1 & \cdots & 0 \\ \vdots & \vdots & \ddots & \vdots \\ 0 & \cdots & 0 & 1 \end{bmatrix}_{N^2\times N^2}, \qquad \boldsymbol{W}_1 = \begin{Bmatrix} W_{1,1} \\ W_{1,2} \\ \vdots \\ W_{1,N\times N} \end{Bmatrix}.$$

Equation (18) represents a generalized eigenvalue problem for ω^2. By solving the equation for each Bloch vector $\boldsymbol{k}$ in the irreducible region of the first Brillouin zone (referring to figure 1(*b*)), we obtain N^2+1 eigenvalues, ω^2, which can be used to represent the band structures, $\omega\ (\boldsymbol{k})$. The existence of band gap is indicated by the absence of eigenvalues in some frequency ranges. The constitution of band structures by the $\omega\ (\boldsymbol{k})$ method is commonly used in the publications on PCs [30, 31], but such a method can only be used to study and characterize propagating wave modes within the pass bands.

In order to characterize evanescent wave modes inside band gaps, in what follows we attempt to reformulate equation (18) to produce an eigenvalue problem of the form $\boldsymbol{k}(\omega)$, which can be used to calculate complex Bloch vectors for a given frequency so that complex band structures can be obtained. The idea of modifying the traditional PWE formulations to enable the calculation of complex Bloch vectors has been developed in several recent publications on PCs [33–35], where an inhomogeneous periodic medium was treated.

To develop the $\boldsymbol{k}(\omega)$ method, first we assume that the azimuth angle of the Bloch vector $\boldsymbol{k}$ is ϕ, then $\boldsymbol{k}$ can be written as

$$\boldsymbol{k} = (k_x, k_y) = k(\cos\phi, \sin\phi). \tag{20}$$

Hence the elements in matrix ($\boldsymbol{K}$) (see equation (19)) can be expressed by

$$\begin{aligned} [\sum_{j=x,y} (\boldsymbol{k}+\boldsymbol{G})_j^2]^2 &= [(k\cos\phi + mb_{11} + nb_{21})^2 \\ &\quad +(k\sin\phi + mb_{12} + nb_{22})^2]^2 \\ &= \frac{1}{a_1^4}[(ka_1)^2 + \varepsilon_1(ka_1) + \varepsilon_0]^2 \\ &= \frac{1}{a_1^4}[(ka_1)^4 + \chi_3(ka_1)^3 + \chi_2(ka_1)^2 + \chi_1(ka_1) + \chi_0], \end{aligned} \tag{21}$$

where

$$\varepsilon_0 = [(mb_{11} + nb_{21})a_1]^2 + [(mb_{12} + nb_{22})a_1]^2,$$
$$\varepsilon_1 = 2[(mb_{11} + nb_{21})a_1 \cos\varphi + (mb_{12} + nb_{22})a_1 \sin\varphi], \quad (22)$$
$$\chi_0 = \varepsilon_0^2,\ \chi_1 = 2\varepsilon_0\varepsilon_1,\ \chi_2 = 2\varepsilon_0 + \varepsilon_1^2,\ \chi_3 = 2\varepsilon_1.$$

Then the matrix $[\boldsymbol{K}]$ can be written as

$$[\boldsymbol{K}] = \frac{1}{a_1^4}\{(ka_1)^4[\boldsymbol{I}] + (ka_1)^3[\boldsymbol{K}_3] + (ka_1)^2[\boldsymbol{K}_2] + (ka_1)[\boldsymbol{K}_1] + [\boldsymbol{K}_0]\}, \quad (23)$$

where

$$[\boldsymbol{K}_{j=0,1,2,3}] = \begin{bmatrix} \chi_{j,1} & 0 & \cdots & 0 \\ 0 & \chi_{j,2} & \cdots & 0 \\ \vdots & \vdots & \ddots & \vdots \\ 0 & \cdots & 0 & \chi_{j,N\times N} \end{bmatrix}. \quad (24)$$

By eliminating the term $w_2(\mathbf{0})$ in equation (18), we have

$$(DS[\boldsymbol{K}] - \rho Sh\omega^2[\boldsymbol{I}] + D_{\mathrm{R}}[\boldsymbol{U}])\{\boldsymbol{W}_1\} = \mathbf{0}, \quad (25)$$

where

$$D_{\mathrm{R}} = k_{\mathrm{R}} - \frac{k_{\mathrm{R}}^2}{k_{\mathrm{R}} - \omega^2 m_{\mathrm{R}}} \quad (26)$$

is the dynamic stiffness of the resonator. Such an expression can also be derived from the following governing equation of the resonator:

$$\left(\begin{bmatrix} k_{\mathrm{R}} & -k_{\mathrm{R}} \\ -k_{\mathrm{R}} & k_{\mathrm{R}} \end{bmatrix} - \omega^2 \begin{bmatrix} 0 & 0 \\ 0 & m_{\mathrm{R}} \end{bmatrix}\right) \begin{Bmatrix} w_1(\mathbf{0}) \\ w_2(\mathbf{0}) \end{Bmatrix} = \begin{Bmatrix} -f_1(\mathbf{0}) \\ 0 \end{Bmatrix}, \quad (27)$$

which gives $-f_1(\mathbf{0}) = D_{\mathrm{R}} w_1(\mathbf{0})$.

Inserting equation (23) into (25) gives

$$(\bar{k}^4[\boldsymbol{I}] + \bar{k}^3[\boldsymbol{K}_3] + \bar{k}^2[\boldsymbol{K}_2] + \bar{k}[\boldsymbol{K}_1] + [\boldsymbol{K}_0] - \bar{k}_{\mathrm{P}}^4[\boldsymbol{I}] + \bar{D}_{\mathrm{R}}[\boldsymbol{U}])\{\boldsymbol{W}_1\} = \mathbf{0}, \quad (28)$$

where

$$\bar{k} = ka_1, \quad \bar{k}_{\mathrm{P}}^4 = (k_{\mathrm{P}}a_1)^4 = \frac{\rho hS\omega^2}{DS/a_1^4}, \quad \bar{D}_{\mathrm{R}} = \frac{D_{\mathrm{R}}}{DS/a_1^4}. \quad (29)$$

For the sake of brevity, we write equation (28) as

$$[\bar{k}^4\boldsymbol{I} + \bar{k}^3\boldsymbol{A}_3 + \bar{k}^2\boldsymbol{A}_2 + \bar{k}\boldsymbol{A}_1 + \boldsymbol{A}_0]\{\boldsymbol{W}_1\} = 0 \quad (30)$$

with

$$\boldsymbol{A}_{1,2,3} = [\boldsymbol{K}_{1,2,3}], \qquad \boldsymbol{A}_0 = [\boldsymbol{K}_0] - \bar{M}_1[\boldsymbol{I}] + \bar{D}_{\mathrm{R}}[\boldsymbol{U}]. \quad (31)$$

Equation (30) is a quadratic eigenvalue problem for $\bar{k} = ka_1$. The problem can be recast as the standard linear eigenvalue problem

$$\begin{bmatrix} -\boldsymbol{A}_3 & -\boldsymbol{A}_2 & -\boldsymbol{A}_1 & -\boldsymbol{A}_0 \\ \boldsymbol{I} & \mathbf{0} & \mathbf{0} & \mathbf{0} \\ \mathbf{0} & \boldsymbol{I} & \mathbf{0} & \mathbf{0} \\ \mathbf{0} & \mathbf{0} & \boldsymbol{I} & \mathbf{0} \end{bmatrix} \begin{Bmatrix} \bar{k}^3\boldsymbol{W}_1 \\ \bar{k}^2\boldsymbol{W}_1 \\ \bar{k}\boldsymbol{W}_1 \\ \boldsymbol{W}_1 \end{Bmatrix} = \bar{k} \begin{Bmatrix} \bar{k}^3\boldsymbol{W}_1 \\ \bar{k}^2\boldsymbol{W}_1 \\ \bar{k}\boldsymbol{W}_1 \\ \boldsymbol{W}_1 \end{Bmatrix}. \quad (32)$$

For a given frequency ω and an azimuth angle ϕ of the Bloch wave vector, equation (32) has $4 \times N^2$ solutions for $\bar{k}$, with possibly complex values, and the associated Bloch wave vectors are determined by equation (20), i.e. $\boldsymbol{k} = (\cos\phi, \sin\phi)\bar{k}/a_1$. In contrast to the $\omega(\boldsymbol{k})$ method represented by equation (18), the formulation of equation (32) provides a $\boldsymbol{k}(\omega)$ method that can be employed to calculate complex band structures. It should be pointed out that, for a given frequency, although $4 \times N^2$ solutions of $\boldsymbol{k}$ can be obtained by equation (32), the lowest component whose real part $\mathrm{Re}(\boldsymbol{k})$ lies inside and around the first Brillouin zone is the most accurate one. Thus, in the numerical examples of the following section, we will present only the results associated with the lowest component.

3. Examples and discussion

3.1. Wave band structure of infinite systems

In this subsection, we focus on the demonstration of flexural wave band gaps in infinite LR plate systems, and in the following subsection, we will examine the vibration transmission through finite LR plate structures to illustrate the vibration attenuation properties within the band gaps.

Two examples of the LR plate systems are considered with the same choices of the plate, lattice constant and resonator mass. The parameters are as follows: $E = 70\,\mathrm{GPa}$, $\nu = 0.3$, $\rho = 2700\,\mathrm{kg\,m^{-3}}$, $h = 0.002\,\mathrm{m}$, $a_1 = a_2 = a = 0.1\,\mathrm{m}$, $m_{\mathrm{R}} = 0.027\,\mathrm{kg}$. Thus, the ratio of the resonator mass to the mass of the plate is $\gamma = m_{\mathrm{R}}/\rho hS = 0.5$. The resonator springs used in the two examples are different. In the first example, the spring constant is chosen as $k_{\mathrm{R}} = 9.593 \times 10^4\,\mathrm{N\,m^{-1}}$, thus the resonant frequency of the resonators is $f_{\mathrm{R}} = (1/2\pi)(k_{\mathrm{R}}/m_{\mathrm{R}})^{1/2} = 300\,\mathrm{Hz}$. In the second example, the spring constant is $k_{\mathrm{R}} = 1.925\times10^5\,\mathrm{N\,m^{-1}}$, i.e. the resonant frequency is tuned to $f_{\mathrm{R}} = 425\,\mathrm{Hz}$.

Figure 2 shows the real band structures calculated by equation (18) for the two LR plate systems (solid lines) mentioned above. In the calculation, we have used $N = (2 \times 4{+}1)^2 = 81$ plane waves. Several calculations were performed to achieve a good convergence of the solutions. The results indicate that both LR plate systems exhibit two directional band gaps (labelled by '$\mathbf{g}_{1,2}$') along the ΓX direction and a complete band gap (labelled by '$\boldsymbol{G_I}$'). The location of gap $\mathbf{g}_1$ is different in the two systems since it is governed by the local resonances. In contrast, the position of gap $\mathbf{g}_2$ remains unchanged because its lower gap edge is determined by the Bragg condition along the ΓX direction (i.e. $a = \lambda_{\mathrm{P}}/2$), which gives the Bragg frequency:

$$f_{\mathrm{B}} = \frac{1}{2\pi}\left(\frac{\pi}{a}\right)^2\sqrt{\frac{D}{\rho h}}. \quad (33)$$

The Bragg frequency has no reference to the properties of local resonators, and for the systems considered here we can calculate that $f_{\mathrm{B}} = 484\,\mathrm{Hz}$. We also observe that the location of the complete gap $\boldsymbol{G_I}$ is almost the same as that of $\mathbf{g}_1$ since it is dominated by the local resonances. Thus, we refer to gaps $\mathbf{g}_1$ and $\boldsymbol{G_I}$ as resonance gaps, but regard gap $\mathbf{g}_2$ as a Bragg gap.

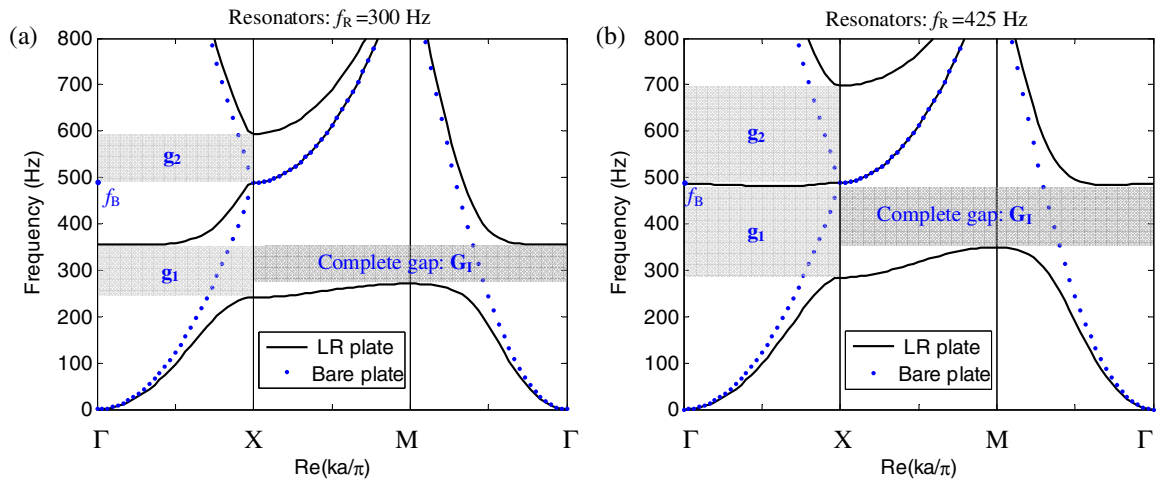

Figure 2. Real band structures calculated by equation (18) for two LR plate systems (solid lines) containing different local resonators: (*a*) $f_R = 300$ Hz, (*b*) $f_R = 425$ Hz. For a comparison, the band structure of the bare plate without resonators (dotted lines) is also shown in the figure. The parameters of the plate, the lattice constant and the resonator masses in the two LR plate systems are identical. '$\mathbf{g}_{1,2}$' and 'G_I' denote directional band gaps and a complete band gap, respectively.

In figure 2, the band structure of the bare plate (dotted lines) is also shown for a comparison. Such a band structure (dotted lines) is obtained using the same PWE formulations as the LR plates but, at the same time, by assuming that the mass of the resonators m_R is extremely small (e.g. $m_R = 1 \times 10^{-15}$ kg) and the resonant frequency of the resonators is considerably high (e.g. $f_R = 5000$ Hz). It is seen that in the XM direction the band structure points of the bare plate lie exactly on top of one band of the LR plates. Such a result is obtained for the bare plate due to the artificial periodic condition that is applied to the bare plate in the PWE formulations. The overlapped band in the XM direction actually represents the evolution of Bragg frequencies with changing wave directions (described by the azimuth angle ϕ). These frequencies are governed by the Bragg conditions along different directions (i.e. $a = \lambda_P/2\cos(\phi)$), which gives

$$f_B(\phi) = \frac{1}{2\pi}\left(\frac{\pi}{a \cdot \cos\phi}\right)^2 \sqrt{\frac{D}{\rho h}}. \tag{34}$$

In the calculation of band structures, the Bloch wave vector $\boldsymbol{k}$ is scanned along the XM direction where $k_x = \pi/a$ and $0 < k_y < \pi/a$; thus for a given calculation point in the XM direction (represented by an assigned k_y), the associated azimuth angle of the Bloch wave vector is $\phi = \text{atan}[k_y/(\pi/a)]$, and thus the corresponding Bragg frequency is given by

$$f_B(k_y) = \frac{1}{2\pi}\left(\frac{\pi}{a \cdot \cos\{\text{atan}[k_y/(\pi/a)]\}}\right)^2 \sqrt{\frac{D}{\rho h}}. \tag{35}$$

Equation (35) represents the analytical solutions of eigenfrequencies on the overlapped band in the XM direction as a function of the assigned k_y in this direction. The lower limit of the solutions is $f_B(k_y = 0)$, which is exactly equal to the Bragg frequency f_B observed at the X point (also see equation (33)). It is evident that all the Bragg frequencies given by equation (35) depend on the lattice constant a, but have no reference to the resonator parameters. Thus, such a Bragg frequency band in the XM direction cannot be affected by tuning the resonant frequency of the resonators, as can be seen from figure 2.

It is interesting to note that, for the case shown in figure 2(*b*), as the resonant frequency of the resonators is tuned to $f_R = 425$ Hz, both the width of the resonance gap $\mathbf{g}_1$ and that of the Bragg gap $\mathbf{g}_2$ are significantly broadened, and the two gaps are nearly coupled together, forming a super-wide pseudo-gap within which only a very narrow pass band exists. The behaviour is very similar to the phenomenon of band gap coupling observed in some one-dimensional (1D) LR systems [36, 37].

In order to demonstrate what is particular about the second resonant frequency (i.e. $f_R = 425$ Hz) that leads to the super-wide pseudo-gap, in figure 3(*a*) we show the maps of the two directional gaps $\mathbf{g}_1$ and $\mathbf{g}_2$ as a function of the resonant frequency f_R. It is seen that when the resonant frequency is tuned to 425 Hz the width of the pass band between these two gaps becomes the narrowest. Such a narrow pass band is almost invisible in comparison with the two wide gaps, and thus a pseudo-gap formed by a combination of gaps $\mathbf{g}_1$ and $\mathbf{g}_2$ arises.

Figure 3(*a*) clearly shows the influence of the resonant frequency on the position of the two directional gaps. When the resonant frequency f_R is tuned within a low-frequency range ($f_R < 425$ Hz), the position of the first gap $\mathbf{g}_1$ increases with increasing f_R, but the location of the second gap $\mathbf{g}_2$ remains unchanged. It is seen that the lower gap edge frequency of $\mathbf{g}_2$ is precisely equal to the Bragg frequency $f_B = 484$ Hz. Thus, in the low-frequency tuning range ($f_R < 425$ Hz), the first gap $\mathbf{g}_1$ can be regarded as a resonance gap while the second gap $\mathbf{g}_2$ can be considered as a Bragg gap. This point is the same as mentioned previously. However, in a higher frequency tuning range (425 Hz $< f_R <$ 600 Hz), the nature of the two gaps seems to be exchanged. As the resonant frequency is tuned to be somewhat higher than 425 Hz, the first gap $\mathbf{g}_1$ becomes a Bragg gap since its upper gap edge always locates at the Bragg

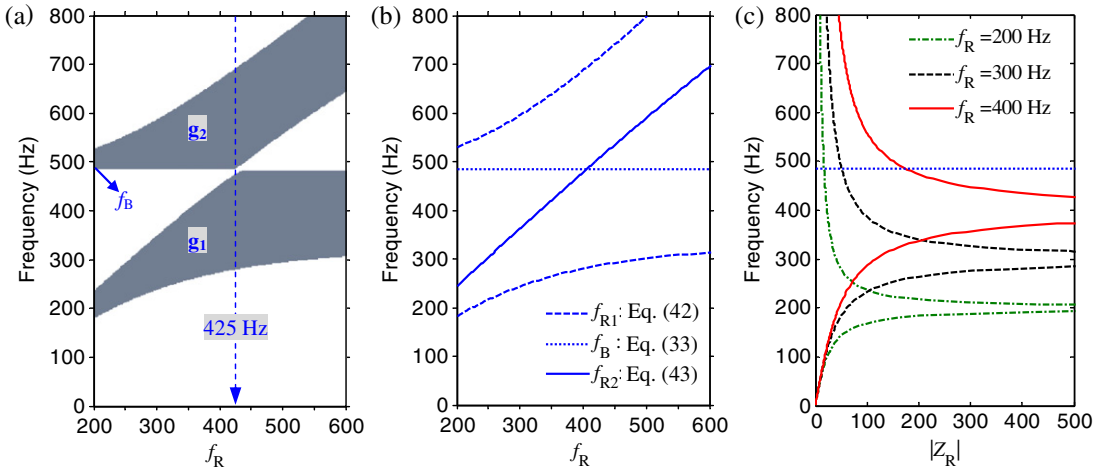

Figure 3. (*a*) Maps of the two directional gaps $\mathbf{g}_1$ and $\mathbf{g}_2$ as a function of the resonant frequency f_R. The parameters of the plate, the lattice constant and the resonator masses are all fixed, and they are chosen to be the same as in figure 2. (*b*) Analytically calculated BEFs based on an approximate model of the system considered in (*a*). (*c*) Evolution of the magnitude of the mechanical input impedance of the resonators ($|Z_R|$) with increasing resonant frequency f_R.

frequency $f_B = 484$ Hz, but the second gap behaves like a resonance gap since its position can be significantly changed by tuning the resonant frequency f_R. The phenomenon observed here is very similar to that of a 1D LR system [37].

In order to achieve a more feasible understanding of the evolution of directional-gap maps shown in figure 3(*a*), we approximate the 2D periodic system as a 1D periodic system consisting of the plate with periodic line resonators lying along the y-direction at the x-wise interval a. The stiffness of the line resonators is k_R/a per unit length and the mass of the line resonators is m_R/a per unit length. Thus, the approximate system is a 2D LR plate with 1D periodicity along the x-direction. Since we consider wave propagation only along the x-direction, the approximate system can be treated in a similar way as that for a 1D LR beam system [23]. Using a transfer matrix method [23], an analytical dispersion relation of the approximate system can be derived as

$$\cosh^2(\mathrm{i}ka) + \alpha_1 \cosh(\mathrm{i}ka) + \alpha_2 = 0, \tag{36}$$

where

$$\begin{aligned}\alpha_1 &= -[\cos(k_P a) + \cosh(k_P a)] - (P/4)[\sin(k_P a) \\ &\quad - \sinh(k_P a)], \\ \alpha_2 &= \cos(k_P a)\cosh(k_P a) + (P/4)[\sin(k_P a)\cosh(k_P a) \\ &\quad - \sinh(k_P a)\cos(k_P a)], \\ P &= D_R/[(D/a^2)(k_P a)^3].\end{aligned} \tag{37}$$

The expression for D_R has been presented in equation (26), and it can be rewritten as a function of the resonant frequency f_R:

$$D_R = \frac{m_R}{1/(2\pi f_R)^2 - 1/(2\pi f)^2}. \tag{38}$$

Similar to some 1D periodic systems [37, 38], the band edges (intersections of the pass bands and the boundaries of the irreducible Brillouin zone, i.e. $ka = \pi$ and $ka = 0$) of the approximate system are governed by the equation

$$\cosh(\mathrm{i}ka) = \pm 1. \tag{39}$$

Substituting equation (39) into (36) yields two groups of band edge frequencies (BEFs). The first group is determined by

$$\cos(k_P a) = \pm 1, \tag{40}$$

which gives the Bragg frequencies:

$$f_{B,n} = \frac{1}{2\pi}\left(\frac{n\pi}{a}\right)^2 \sqrt{\frac{D}{\rho h}}, \qquad n = (1, 2, 3, \ldots). \tag{41}$$

The second group can be represented by the following two equations:

$$f_{R1} := \left\{(f_R, f)\,|\,f_R = \frac{1}{2\pi}\left(\frac{1}{(2\pi f)^2} + \frac{m_R[\tanh(k_P a/2) - \tan(k_P a/2)]/4}{(D/a^2)(k_P a)^3}\right)^{-1/2}\right\} \tag{42}$$

and

$$f_{R2} := \left\{(f_R, f)\,|\,f_R = \frac{1}{2\pi}\left(\frac{1}{(2\pi f)^2} + \frac{m_R[\coth(k_P a/2) + \cot(k_P a/2)]/4}{(D/a^2)(k_P a)^3}\right)^{-1/2}\right\}. \tag{43}$$

Note that the Bragg frequency f_B given by equation (33) actually represents the lowest component of those given by equation (41).

Figure 3(*b*) shows the BEF curves obtained analytically by equations (33), (42) and (43). It can be seen that the BEF curves are in good agreement with the band-gap edges shown in figure 3(*a*), especially in the frequency range around and below the Bragg frequency f_B. However, considerable discrepancy can be observed in the higher frequency range. This is expected, since at higher frequencies the spacing between the point resonators, a, is comparable to or smaller than the wavelength of motion in the thin plate. Thus, the effects of the resonator interval along the y-direction should be taken into

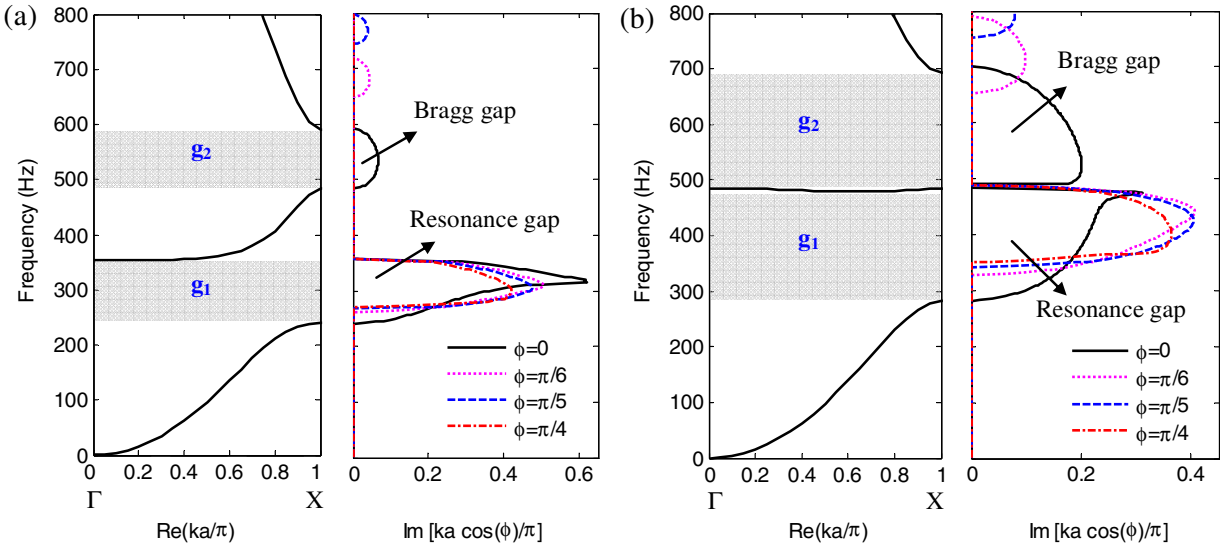

Figure 4. Complex band structures calculated by equation (32) for the two LR plate systems considered in figure 2: (*a*) $f_R = 300$ Hz, (*b*) $f_R = 425$ Hz. In the left panels of (*a*) and (*b*), only the solutions along the ΓX direction ($\phi = 0$) are shown, but in the right panels, the solutions along four different directions are depicted for comparison. The case of $\phi = \pi/4$ represents the ΓM direction.

account to address the plate wave motion. But such effects are neglected in the approximate model, where line resonators lying along the y-direction are adopted. Accordingly, the approximation is not accurate in the high-frequency range.

It is worth noting that the overlap of the BEF curves f_B and f_{R2} in figure 3(*b*) can provide a close approximation to the condition under which the resonant frequency should be tuned to achieve a pseudo-gap. The approximate condition can be obtained by inserting the relation $f = f_B$ (i.e. $k_P a = \pi$) into equation (43), which yields

$$f_R = \frac{1}{2\pi}\left(\frac{\rho h a^4}{D\pi^4} + \frac{m_R a^2}{D\pi^3}\frac{\coth(\pi/2)}{4}\right)^{-1/2}. \qquad (44)$$

This represents an initial design formula to determine the resonant frequency that leads to a wide pseudo-directional gap. For the system considered in figure 3(*a*), using equation (44) we can calculate that $f_R = 405$ Hz, which is a good approximation to the true condition $f_R = 425$ Hz.

Figure 3(*a*) also indicates that the width of the two directional gaps can be significantly broadened by increasing the resonant frequency f_R in the low-frequency tuning region ($f_R < 425$ Hz). To gain a physical insight into the gap broadening effects, we examine the mechanical input impedance (the ratio of the driving force to the resultant speed at the attachment point) of the resonators, denoted by Z_R. The magnitude of Z_R can be written as

$$|Z_R| = \left|\frac{D_R}{i\omega}\right|. \qquad (45)$$

Figure 3(*c*) shows the evolution of $|Z_R|$ with increasing resonant frequency f_R. It is seen that the curve of $|Z_R|$ always has a peak value at the resonant frequency and falls at lower and higher frequencies. For a resonator with a higher f_R, the curve of $|Z_R|$ falls off more slowly around the resonant frequency, and thus the resonator has a broader resonance, giving rise to a broader band of impedance mismatch near the resonant frequency in the LR plate system. This explains why the size of the resonance-type gap $\mathbf{g}_1$ increases as f_R is tuned within the low-frequency region (e.g. $f_R < 425$ Hz). On the other hand, figure 3(*c*) also demonstrates that, as the resonant frequency f_R is increased, the impedance magnitude $|Z_R|$ at the Bragg frequency f_B is also increased, thus the Bragg scattering induced by the periodic impedance mismatch is intensified. This provides an idea to understand the broadening of the Bragg-type gap $\mathbf{g}_2$ as f_R is tuned in the low-frequency range. It should be noted that, if the resonant frequency is tuned close to or higher than the condition $f_R = 425$ Hz, the band gap formation is more complicated and the evolution of gap width may not be simply understood by the change in the resonator impedance. More careful discussions of the associated gap formation mechanisms may be the subject of a future work.

Figure 4 shows the complex band structures calculated by equation (32) for the two example systems considered in figure 2. The number of plane waves used in the calculation is the same as previous examples, i.e. $N = (2\times4+1)^2 = 81$. The left panels of figures 4(*a*) and (*b*) display the purely real Bloch wave vectors (whose imaginary part satisfies $\mathrm{Im}(k) = 0$). For a clear illustration, in the left panels, we present only the solutions along the ΓX direction ($\phi = 0$). As expected, the real band structures (along the ΓX direction) shown in figure 4 agree very well with those presented in figure 2. The right panels of figures 4(*a*) and (*b*) show the imaginary part of the Bloch wave vector whose absolute value, $|\mathrm{Im}(k)|$, is the smallest one among all the solutions. It is worth noting that the wave attenuation property inside a band gap is mostly quantified by the value of the smallest $|\mathrm{Im}(k)|$, since it represents the least rapidly decaying wave (evanescent Bloch wave [33–35]) that carries energy the farthest. Consequently, the results shown in the right panels of figures 4(*a*) and (*b*) present good descriptions of the band gap behaviour since they simultaneously show the location, width and attenuation

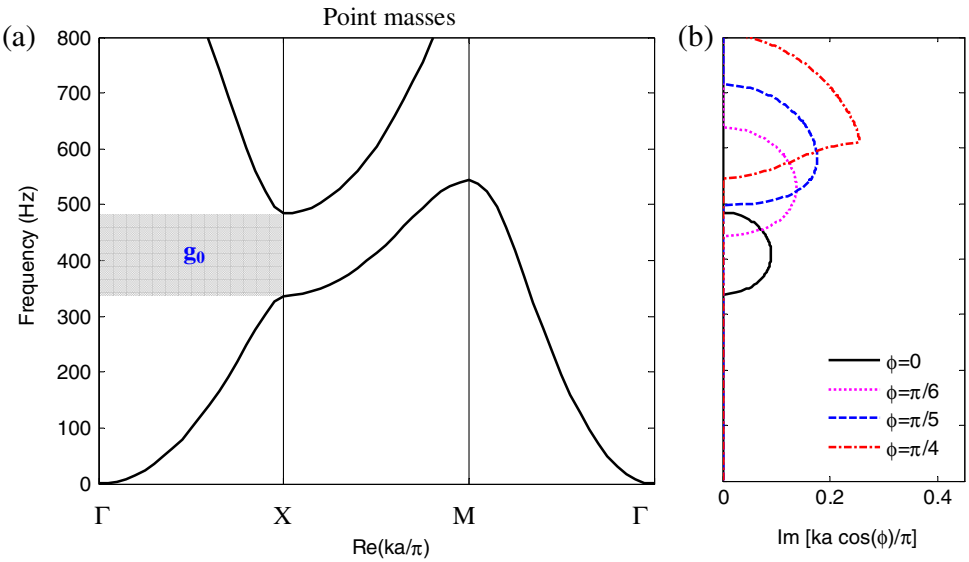

Figure 5. Complex band structures for a periodic system made of a thin plate with periodically attached point masses: (*a*) the real wave band structure, (*b*) the imaginary part of Bloch wave vectors. The parameters of the plate, the lattice constant and the masses are all the same as in figures 2 and 4. Note that along the ΓX direction only a Bragg gap $\mathbf{g}_0$ exists. Moreover, no complete band gap is achieved in the system.

performance of all the band gaps in the frequency range considered.

Two additional features can be observed in the right panels of figures 4(*a*) and (*b*). First, the attenuation properties of the two gaps $\mathbf{g}_1$ and $\mathbf{g}_2$ are very different from each other. It is shown that gap $\mathbf{g}_1$ is always characterized by a sharp maximum attenuation, but gap $\mathbf{g}_2$ displays a considerably smooth profile of attenuation over the gap range. This further confirms that $\mathbf{g}_1$ is a resonance gap while $\mathbf{g}_2$ is a Bragg gap. Such a distinction between the attenuation properties of resonance and Bragg gaps has been observed commonly in the previous studies of LR periodic systems [4, 6, 9, 37]. Second, we can see that the location of the Bragg gap $\mathbf{g}_2$ gradually moves to a higher frequency range when the azimuth angle ϕ is increased from 0 to $\pi/4$. This can be explained by the Bragg conditions along different directions (i.e. $a = \lambda_P/2\cos(\phi)$), which gives the Bragg frequencies $f_B(\phi)$ (see equation (34)). For the cases $\phi = \pi/6$, $\pi/5$ and $\pi/4$, we can respectively calculate that $f_B(\phi) = 645.4$ Hz, 739.6 Hz and 968.1 Hz. It can be seen that the location of the Bragg gaps $\mathbf{g}_2$ along different directions (ϕ) can be approximated well by the associated Bragg frequencies $f_B(\phi)$.

In order to demonstrate the advantage of the LR plate systems, we also calculate the band structure for a conventional periodic system made of a thin plate with periodically attached point masses. We refer to such a periodic plate system as the masses-loaded (ML) plate system. For a direct comparison, the parameters of the plate, the lattice constant and the masses of the ML plate system are chosen to be the same as the LR plates considered in figures 2 and 4. The band structure of the ML plate system can be calculated by employing the same formulations as the LR plates but supposing the spring constant to be extremely large (e.g. $k_R = 1 \times 10^{12}\,\mathrm{N\,m^{-1}}$), thus the masses are almost rigidly attached to the plate. The calculated band structure of the ML plate is shown in figure 5. As previously, $N = (2\times4+1)^2 = 81$ plane waves are used in the calculation. Figure 5 indicates that along the ΓX direction only one directional Bragg gap $\mathbf{g}_0$ is achieved in the ML plate system. We also find that the band width of such a Bragg gap $\mathbf{g}_0$ is much narrower than the gap $\mathbf{g}_1$ shown in figure 4(*b*), and in addition, the attenuation performance (quantified by $|\mathrm{Im}(k)|$) of gap $\mathbf{g}_0$ is much lower than that of $\mathbf{g}_1$ shown in figure 4(*b*). Furthermore, no complete band gap is achieved in the present ML plate system. The comparisons clearly indicate the advantage of the LR plate systems in forming broader band gaps as well as in achieving higher wave attenuation performance inside the band gaps. Another disadvantage of the ML plate system is that the location of the directional gap $\mathbf{g}_0$ is governed by the Bragg condition (see equation (33)), thus, to achieve such a gap at a very low frequency, a very large lattice constant is required. In contrast, for the LR plate, the location of the directional gap $\mathbf{g}_1$ can be easily adjusted by tuning the resonant frequency f_R, as shown in figure 3(*a*).

3.2. *Vibration transmittance of finite structures*

Vibration transmission through finite LR plates is of particular interest since plate structures are generally finitely sized in practice. As an illustration, we consider two finite LR plates made of 10×10 unit cells; the parameters are identical to the two examples considered in figure 2. We adopt the well-known finite element method to calculate the vibration transmittance of such finite structures, and the finite element model is sketched in figure 6. In the figure, the notation 'excitation 1/2' represents a line/point harmonic displacement excitation, and 'point 1/2' denotes the location on the plate where the transverse vibration responses are of interest. We assume that the excitation and the response function are respectively represented by $q_{ext}\exp(i\omega t)$ and $q_{res}\exp(i\omega t)$. Then the transverse vibration transmittance of the finite LR plate is given by $T = |q_{res}/q_{ext}|$.

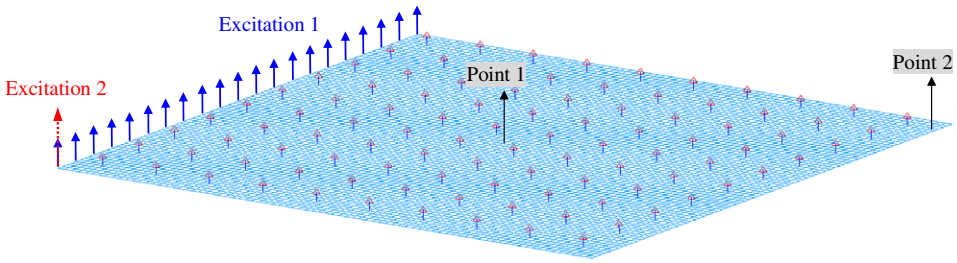

Figure 6. Finite element model of a LR plate with 10 × 10 unit cells. 'Excitation 1/2' represents a line/point harmonic displacement excitation. The vibration transmittances at points 1 and 2 are calculated.

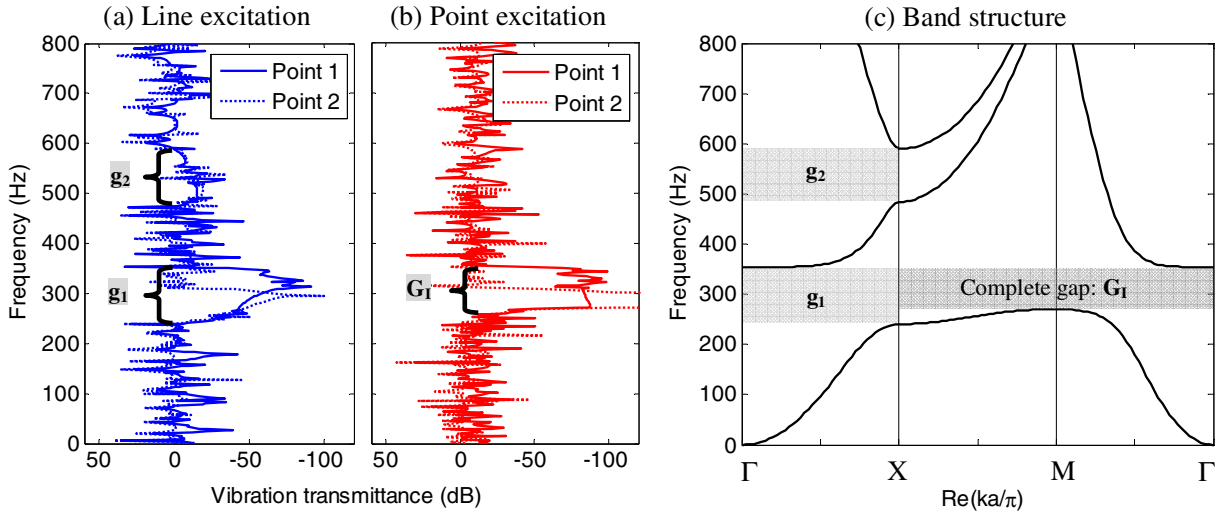

Figure 7. Vibration transmittance of the finite LR plate ($f_R = 300$ Hz) corresponding to the case considered in figure 2(a) under (a) line excitation and (b) point excitation. For ease of comparison, the band structure of the infinite system, which has been shown in figure 2(a), is replotted here in (c). The location and width of the transmission gaps revealed by the solid lines in (a) and (b) are in good agreement with the band gaps shown in (c).

Figures 7(a) and (b) show the vibration transmittance of the finite LR plate structure ($f_R = 300$ Hz) associated with the example considered in figure 2(a). The transmittance curves for the case of line excitation are depicted in figure 7(a). Two transmission gaps can be observed. This is due to the existence of two directional band gaps (see $\mathbf{g}_1$ and $\mathbf{g}_2$ in figure 7(c)) along the ΓX direction and the line excitation is more likely to produce plane waves propagating along the ΓX direction. Figure 7(a) also indicates that the transmission gaps revealed by the solid line (point 1) match better with the band gaps shown in figure 7(c) than those revealed by the dotted line (point 2). In particular, the vibration transmittance at point 2 (dotted line) can be very large even at some frequencies (e.g. at 320 Hz) inside the region of the band gap $\mathbf{g}_1$. This may be understood by the steady-state wave profile of the finite structure, which will be presented later. Figure 7(a) also shows that the maximum transmission drop inside gap $\mathbf{g}_1$ is much larger than that in gap$\mathbf{g}_2$. This can be explained by the imaginary parts of the Bloch wave vectors presented in the right panel of figure 4(a), which imply that the attenuation performance of the resonance gap $\mathbf{g}_1$ is much higher than the Bragg gap $\mathbf{g}_2$. Figure 7(b) further shows the transmittance curves for the case of point excitation. Since the point excitation can trigger waves propagating along all directions, the transmission gap shown in figure 6(b) originates from the complete gap $\boldsymbol{G_I}$ shown in figure 7(c).

Figure 8 shows several steady-state wave profiles of the finite LR plate structure considered in figure 7. Three specific frequencies are considered. The frequency '200 Hz' locates inside the pass band, thus the produced waves can propagate through the entire structure without attenuation (see figures 8(a_1) and (b_1)). The frequency '320 Hz' lies inside both the directional gap $\mathbf{g}_1$ and the complete gap $\boldsymbol{G_I}$, therefore waves are expected to be attenuated after propagating across several unit cells of the periodic structure. Figures 8(a_2) and (b_2) show that the excited waves are significantly suppressed in the interior area of the structure, but can still propagate along the edges of the structure without significant attenuation. This may be due to the free boundary effects of the finite structure (no external constraints are applied to the structural edges except the displacement excitations denoted in figure 6). A more careful discussion of the relationship between such wave profiles (see figures 8(a_1) and (b_1)) of the finite structure and the Bloch wave modes of the infinite system is deferred to a future work. Moreover, the frequency '550 Hz' locates inside the directional gap $\mathbf{g}_2$, therefore for the case of line excitation (see figures 8(a_3)), the produced plane waves (along the ΓX direction) are gradually attenuated along the

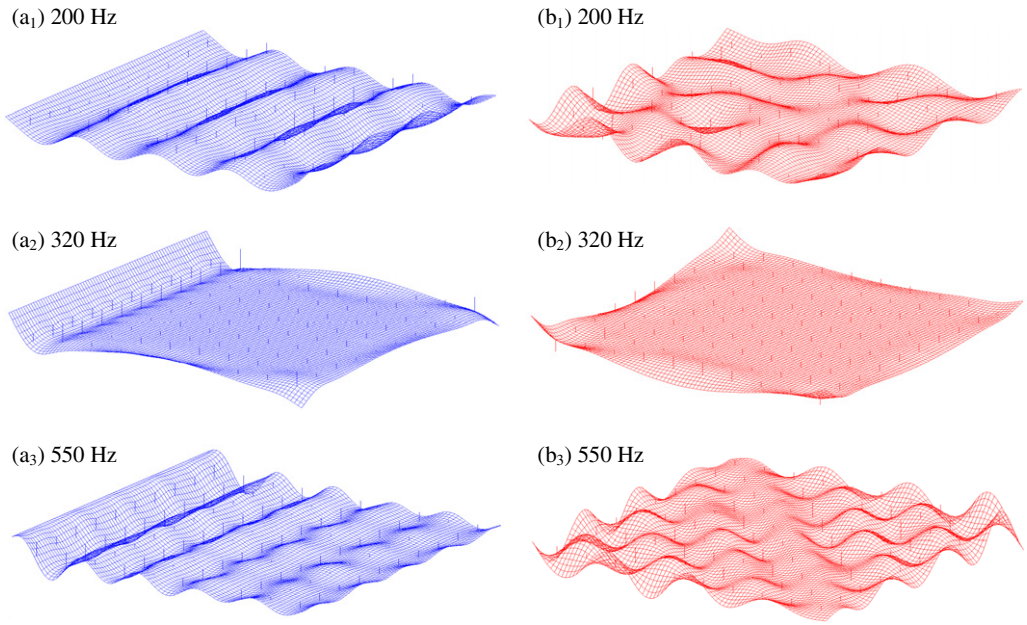

Figure 8. Steady-state wave profiles of the finite LR plate considered in figure 7: (a_1)–(a_3) line excitation, (b_1)–(b_3) point excitation. Note that, at a frequency of 320 Hz (inside the gaps $\mathbf{g}_1$ and $\boldsymbol{G_I}$), the excited waves can propagate without considerable attenuation along the free edges of the finite structure, but are significantly suppressed in the interior area of the structure.

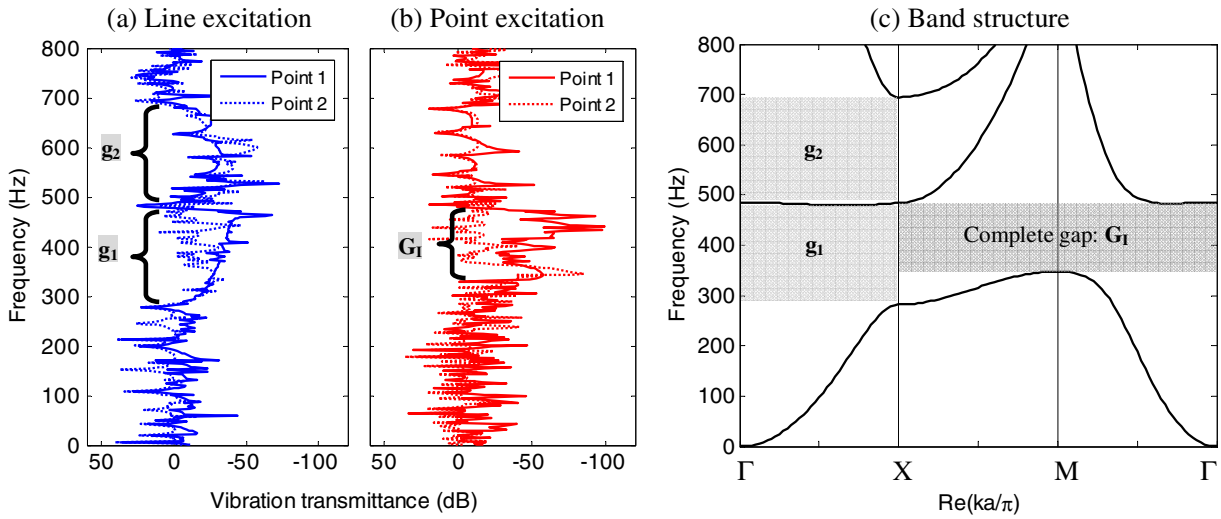

Figure 9. The same as in figure 7, but for the finite LR plate ($f_R = 425$ Hz) corresponding to the case considered in figure 2(b). The regions of the vibration transmission gaps revealed by the solid lines in (a) and (b) match well with the band gaps shown in (c).

propagation direction. But for the case of point excitation (see figures 8(b_3)), no significant wave attenuation can be observed since many waves that can propagate freely along other directions are excited.

Figures 9(a) and (b) show the vibration transmittance of the finite LR plate structure ($f_R = 425$ Hz) corresponding to the case considered in figure 2(b). For a direct comparison, the band structure which has been shown in figure 2(b) is replotted here in figure 9(c). In addition, figure 10 shows the steady-state wave profiles of the finite LR plate structure at some particular frequencies. Similar conclusions can be drawn from figures 9 and 10 as previously (i.e. as from figures 7 and 8). However, some distinctions are clearly seen. It is seen that a narrow region with remarkable transmission peaks arises between gaps $\mathbf{g}_1$ and $\mathbf{g}_2$ in figure 9(a). This is due to the existence of a very narrow pass band along the ΓX direction, as shown in figure 9(c). In addition, here the transmission drop inside the Bragg gap $\mathbf{g}_2$ is commonly much larger than the counterpart shown in figure 7(a). This is because the attenuation performance of gap $\mathbf{g}_2$ in this case is much higher than the previous one, as has been demonstrated by the complex band structures in figure 4. Furthermore, figure 9(b) shows that the region of the complete band gap $\boldsymbol{G_I}$ is captured much better by the transmission gap observed at point 1 (solid line) than at point 2 (dotted line), since the free boundary effects can be remarkable at some frequencies inside gap $\boldsymbol{G_I}$. An example is demonstrated in figure 10(b_2).

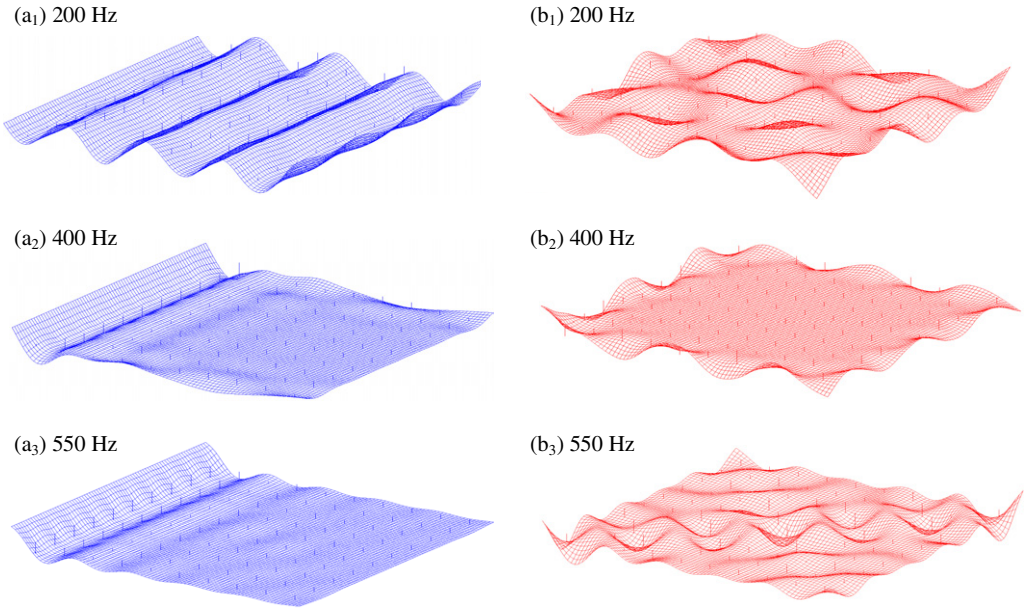

Figure 10. Steady-state wave profiles of the finite LR plate considered in figure 9: (a_1)–(a_3) line excitation, (b_1)–(b_3) point excitation. Note that, at the frequency 400 Hz, the excited waves can propagate along the free structure edges more easily than through the interior area of the structure, as shown in (a_2) and (b_2).

4. Conclusions

In this paper, we have investigated flexural wave propagation and vibration transmission in a LR thin plate with a 2D periodic array of attached spring–mass resonators. The well-known PWE method is extended to deal with such a continuous plate system containing periodic lumped resonant elements. Rather simple and explicit matrix formulations are derived for the calculation of wave band structures. In particular, a $\boldsymbol{k}(\omega)$ method is developed to predict the imaginary part of Bloch wave vectors, Im($\boldsymbol{k}$), which can be used to quantify the wave attenuation performance of band gaps.

It is shown that resonance-type and Bragg-type band gaps coexist in the LR plate due to the coexistence of local resonance and structural periodicity. We also find that, by tuning the resonant frequency of the local resonators (the mass of the resonators are fixed at the same time), width of both the resonance gap and Bragg gap can be significantly broadened. In a special situation, a super-wide pseudo-directional gap can be formed by a combination of the resonance gap and the Bragg gap; inside such a pseudo-gap, only a very narrow pass band exists. Furthermore, based on an approximate model, an explicit design formula is derived to determine the resonant frequency of the resonators that leads to a wide pseudo-gap. We further examined vibration transmission in finite LR plates using the finite element method. Vibration transmission gaps are observed from the transmittance curves of finite LR plates, which confirm the existence of flexural wave band gaps. The position, bandwidth and attenuation behaviour of the transmission gaps match well with the band gap properties displayed in the band structures predicted by the PWE method. We note that the results presented in this paper can facilitate the design and understanding of LR plates, and can find applications in the control of flexural vibration and wave propagation in plates and plate-like structures. Moreover, the PWE formulations developed here can be extended to deal with similar systems with 2D multiple periodic arrays of resonators, in which more wave phenomena and application possibilities can be explored.

Acknowledgments

This work was supported by the National Natural Science Foundation of China (Grant Nos 51075392, 51175501, 50905182 and 10902123). The authors are grateful to the referees for helpful suggestions which improved the paper.

References

[1] Kushwaha M S, Halevi P, Dobrzynski L and Djafari-Rouhani B 1993 *Phys. Rev. Lett.* **71** 2022
[2] Sigalas M, Kushwaha M S, Economou E N, Kafesaki M, Psarobas I E and Steurer W 2005 *Z. Kristallogr.* **220** 765
[3] Pennec Y, Vasseur J O, Djafari-Rouhani B, Dobrzynski L and Deymier P A 2010 *Surf. Sci. Rep.* **65** 229
[4] Liu Z, Zhang X, Mao Y, Zhu Y Y, Yang Z, Chan C T and Sheng P 2000 *Science* **289** 1734
[5] Liu Z, Chan C T and Sheng P 2002 *Phys. Rev.* B **65** 165116
[6] Goffaux C, Sánchez-Dehesa J, Yeyati A L, Lambin P, Khelif A, Vasseur J O and Djafari-Rouhani B 2002 *Phys. Rev. Lett.* **88** 225502
[7] Wang G, Wen X, Wen J, Shao L and Liu Y 2004 *Phys. Rev. Lett.* **93** 154302
[8] Hsu J C and Wu T T 2007 *Appl. Phys. Lett.* **90** 201904
[9] Hsu J C 2011 *J. Phys. D: Appl. Phys.* **44** 055401
[10] Oudich M, Li Y, Assouar B M and Hou Z 2010 *New J. Phys.* **12** 083049
[11] Oudich M, Assouar M B and Hou Z 2010 *Appl. Phys. Lett.* **97** 193503
[12] Oudich M, Senesi M, Assouar M B, Ruzenne M, Sun J H, Vincent B, Hou Z and Wu T T 2011 *Phys. Rev.* B **84** 165136

[13] Wen J, Zhao H, Lv L, Yuan B, Wang G and Wen X 2011 *J. Acoust. Soc. Am.* **130** 1201
[14] Yao Y, Wu F, Zhang X and Hou Z 2012 *Phys. Lett.* A **376** 579
[15] Li J and Chan C T 2004 *Phys. Rev.* E **70** 055602
[16] Milton G W 2007 *New J. Phys.* **9** 359
[17] Huang H H and Sun C T 2011 *J. Mech. Phys. Solids* **59** 2070
[18] Zhu R, Huang G L, Huang H H and Sun C T 2011 *Phys. Lett.* A **375** 2863
[19] Milton G W and Willis J R 2007 *Proc. R. Soc.* A **463** 855
[20] Yao S S, Zhou X M and Hu G K 2008 *New J. Phys.* **10** 043020
[21] Huang H H and Sun C T 2009 *New J. Phys.* **11** 013003
[22] Wang G, Wen X, Wen J and Liu Y 2006 *J. Appl. Mech.* **73** 167
[23] Yu D, Liu Y, Wang G, Zhao H and Qiu J 2006 *J. Appl. Phys.* **100** 124901
[24] Yu D, Wen J, Shen H, Xiao Y and Wen X 2012 *Phys. Lett.* A **376** 626
[25] Liu L and Hussein M I 2012 *J. Appl. Mech.* **79** 011003
[26] Wu T T, Huang Z G, Tsai T C and Wu T C 2008 *Appl. Phys. Lett.* **93** 111902
[27] Pennec Y, Djafari-Rouhani B, Larabi H, Vasseur J O and Hladky-Hennion A C 2008 *Phys. Rev.* B **78** 104105
[28] Wu T T, Hsu J C and Sun J H 2011 *IEEE Trans. Ultrason. Ferroelectr. Freq. Control* **58** 2146
[29] Fahy F and Gardonio P 2007 *Sound and Structural Vibration: Radiation, Transmission and Response* 2nd edn (Oxford: Academic)
[30] Sigalas M M and Economou E N 1994 *J. Appl. Phys.* **75** 2845
[31] Hsu J C and Wu T T 2006 *Phys. Rev.* B **74** 144303
[32] Brillouin L 1946 *Wave Propagation in Periodic Structures* (New York: Dover)
[33] Romero-García V, Sánchez-Pérez J V and Garcia-Raffi L M 2010 *J. Appl. Phys.* **108** 044907
[34] Romero-García V, Sánchez-Pérez J V, Castineira-Ibanez S and Garcia-Raffi L M 2010 *Appl. Phys. Lett.* **96** 124102
[35] Romero-García V, Sánchez-Pérez J V and Garcia-Raffi L M 2010 *New J. Phys.* **12** 083024
[36] Yu D, Wen J, Zhao H, Liu Y and Wen X 2008 *J. Sound Vib.* **318** 193
[37] Xiao Y, Mace B R, Wen J and Wen X 2011 *Phys. Lett.* A **375** 1485
[38] Mead D J 1975 *J. Sound Vib.* **40** 1